

EUROPEAN ORGANIZATION FOR NUCLEAR RESEARCH

CERN-EP/99-17
February 11, 1999

Measurement of Mass and Width of the W Boson at LEP

The L3 Collaboration

Abstract

We report on measurements of the mass and total decay width of the W boson with the L3 detector at LEP. W-pair events produced in e^+e^- interactions between 161 GeV and 183 GeV centre-of-mass energy are selected in a data sample corresponding to a total luminosity of 76.7 pb^{-1} . Combining all final states in W-pair production, the mass and total decay width of the W boson are determined to be $M_W = 80.61 \pm 0.15 \text{ GeV}$ and $\Gamma_W = 1.97 \pm 0.38 \text{ GeV}$, respectively.

Submitted to *Phys. Lett. B*

1 Introduction

For the 1997 data taking period, the centre-of-mass energy, \sqrt{s} , of the e^+e^- collider LEP at CERN was increased to 183 GeV. This energy is well above the kinematic threshold of W-boson pair production, $e^+e^- \rightarrow W^+W^-$.

Analysis of W-pair production yields important knowledge about the Standard Model of electroweak interactions [1] through the measurements of the mass, M_W , and the total decay width, Γ_W , of the W boson [2]. These parameters were initially measured at $p\bar{p}$ colliders [3,4].

First direct measurements of M_W in e^+e^- collisions were derived from total cross section measurements [5–9], mainly at the kinematic threshold of the reaction $e^+e^- \rightarrow W^+W^-$, $\sqrt{s} = 161$ GeV, where the dependence of the W-pair cross section on the W-boson mass is largest. At centre-of-mass energies well above the kinematic threshold, the mass and also the total width of the W boson are determined by analysing the invariant mass of the W-boson decay products [10–13].

In this letter we report on an improved determination of the mass and the total width of the W boson. The analysis is based on the data sample collected in the year 1997 at an average centre-of-mass energy of 183 GeV, corresponding to an integrated luminosity of 55.5 pb^{-1} . The invariant mass distributions of 588 W-pair events selected at this energy are analysed to determine M_W and Γ_W . The results based on the 1997 data are combined with our previously published measurements based on the 1996 data collected at centre-of-mass energies of 161 GeV and 172 GeV [5,6,10].

2 Analysis of Four-Fermion Production

During the 1997 run the L3 detector [14] collected integrated luminosities of 4.04 pb^{-1} , 49.58 pb^{-1} and 1.85 pb^{-1} at centre-of-mass energies of 181.70 GeV, 182.72 GeV and 183.79 GeV, respectively, where these centre-of-mass energies are known to ± 0.05 GeV [15]. These data samples are collectively referred to as 183 GeV data in the following.

The W boson decays into a quark-antiquark pair, such as $W^- \rightarrow \bar{u}d$ or $\bar{c}s$, or a lepton-antilepton pair, $W^- \rightarrow \ell^- \bar{\nu}_\ell$ ($\ell = e, \mu, \tau$); in the following denoted as qq , $\ell\nu$ or ff in general for both W^+ and W^- decays. Four-fermion final states expected in W-pair production are $\ell\nu\ell\nu(\gamma)$, $qq\ell\nu(\gamma)$, and $qqqq(\gamma)$, where (γ) indicates the possible presence of radiative photons.

The following Monte Carlo event generators are used to simulate the signal and background reactions: KORALW [16] and HERWIG [17] ($e^+e^- \rightarrow WW \rightarrow ffff(\gamma)$); EXCALIBUR [18] ($e^+e^- \rightarrow ffff(\gamma)$); PYTHIA [19] ($e^+e^- \rightarrow q\bar{q}(\gamma), ZZ(\gamma)$); KORALZ [20] ($e^+e^- \rightarrow \mu^+\mu^-(\gamma), \tau^+\tau^-(\gamma)$); BHAGENE3 [21], BHWIDE [22] and TEEGG [23] ($e^+e^- \rightarrow e^+e^-(\gamma)$), DIAG36 [24] and LEP4F [25] (leptonic two-photon collisions); PHOJET [26] (hadronic two-photon collisions). The response of the L3 detector is modelled with the GEANT [27] detector simulation program which includes the effects of energy loss, multiple scattering and showering in the detector material.

The selections of the four-fermion final states are described in detail in References 5,6 and 28 for the data collected at $\sqrt{s} = 161$ GeV, 172 GeV and 183 GeV. These analyses reconstruct the visible fermions in the final state, *i.e.*, electrons, muons, τ jets corresponding to the visible τ decay products, and hadronic jets corresponding to quarks. In order to select a pure sample of $qqqq$ events, the cut of 0.67 on the neural-network output described in the $qqqq$ cross-section analysis is applied [28]. Kinematic constraints as discussed below are then imposed to improve

the resolution in the measured fermion energies and angles and to determine those not measured. The invariant mass of the W boson is obtained from its decay products.

The mass and the width of the W boson are determined by comparing samples of Monte Carlo events to the data. A reweighting procedure is applied to construct Monte Carlo samples corresponding to different mass and width values. Using this method, effects of selection and resolution are automatically taken into account.

3 Event Reconstruction imposing Kinematic Constraints

The final states $qqe\nu$, $qq\mu\nu$ and $qqq\nu$ contain at most one primary unmeasured neutrino. For each event a kinematic fit is performed in order to determine energy, E_f , polar angle, θ_f , and azimuthal angle, ϕ_f , for all four fermions, f , in the final state. The kinematic fit adjusts the measurements of these quantities for the visible fermions according to their experimental resolutions to satisfy the constraints imposed, thus improving their resolution.

Four-momentum conservation and equal mass of the two W bosons are imposed as constraints, allowing the determination of the momentum vector of the unmeasured neutrino. For the energy constraint, the exact centre-of-mass energies as given in the previous section are used. For hadronic jets, the velocity $\beta_f = |\vec{p}_f|/E_f$ of the jet is fixed to its measured value as systematic effects cancel in the ratio. For $qqe\nu$ and $qq\mu\nu$ events, this yields a two-constraint (2C) kinematic fit, whereas for $qqq\nu$ events it is a five-constraint (5C) kinematic fit.

Events with badly reconstructed hadronic jets are rejected by requiring that the probability of the kinematic fit exceeds 5%. The kinematic fit mainly improves the energy resolution and less the angular resolution. The resolutions in average invariant mass, m_{inv} , typically improve by a factor of four for $qqe\nu$ and $qq\mu\nu$ events and a factor of six for $qqq\nu$ events.

For $qq\tau\nu$ events, the decay products of the leptonically decaying W boson contain at least two unmeasured neutrinos in the final state. Therefore only the hadronically decaying W boson is used in the invariant mass reconstruction. The energies of the two hadronic jets are rescaled by a common factor so that the sum of their energies equals half the centre-of-mass energy, thus imposing equal mass of the two W bosons. The rescaling improves the resolution in invariant mass by nearly a factor of four. Since invariant masses of W bosons in $\ell\nu\ell\nu$ events cannot be reconstructed as the decay of both W bosons involves neutrinos, $\ell\nu\ell\nu$ events are not used in the analysis for W mass and width.

4 Fitting Method for Mass and Width

The fitting procedure uses the maximum likelihood method to extract values and errors of the W-boson mass M_W , and the total width Γ_W , denoted as Ψ for short in the following. In fits to determine M_W only, the Standard Model relation $\Gamma_W = 3G_F M_W^3 / (2\sqrt{2}\pi)(1 + 2\alpha_S / (3\pi))$ [29] is imposed. Otherwise, M_W and Γ_W are treated as independent quantities.

The kinematic fit imposing the equal-mass constraint determines the weighted average of the two invariant W masses in an event, m_{inv} , which is considered in the fit for mass and width. The total likelihood is the product of the normalised differential cross section, $L(m_{\text{inv}}, \Psi)$, evaluated for all data events. For a given four-fermion final state i , one has:

$$L_i(m_{\text{inv}}, \Psi) = \frac{1}{f_i(\Psi)\sigma_i(\Psi) + \sigma_i^{\text{BG}}} \left[f_i(\Psi) \frac{d\sigma_i(m_{\text{inv}}, \Psi)}{dm_{\text{inv}}} + \frac{d\sigma_i^{\text{BG}}(m_{\text{inv}})}{dm_{\text{inv}}} \right], \quad (1)$$

where σ_i and σ_i^{BG} are the accepted signal and background cross sections and $f_i(\Psi)$ a factor calculated such that the sum of accepted background and reweighted accepted signal cross section coincides with the measured cross section. This way mass and width are determined from the shape of the invariant mass distribution only. The total and differential cross sections of the accepted background are independent of the parameters Ψ of interest. They are taken from Monte Carlo simulations.

The total and differential signal cross sections depend on Ψ . For values Ψ_{fit} varied during the fitting procedure, these cross sections are determined by a reweighting procedure applied to Monte Carlo events originally generated with parameter values Ψ_{gen} . The event weights R_i are given by the ratio:

$$R_i(p_1, p_2, p_3, p_4, k_\gamma, \Psi_{\text{fit}}, \Psi_{\text{gen}}) = \frac{|\mathcal{M}_i^{4\text{F}}(p_1, p_2, p_3, p_4, k_\gamma, \Psi_{\text{fit}})|^2}{|\mathcal{M}_i^{\text{CC03}}(p_1, p_2, p_3, p_4, k_\gamma, \Psi_{\text{gen}})|^2}, \quad (2)$$

where \mathcal{M}_i is the matrix element of the four-fermion final state i . The matrix elements are calculated for the generated four-vectors, $(p_1, p_2, p_3, p_4, k_\gamma)$, of the four fermions and any radiative photons in the event. Since the Monte Carlo sample used for reweighting is based on the three Feynman graphs in W-pair production (CC03 [29–31]), the matrix element in the denominator is calculated using only CC03 graphs. The matrix element in the numerator is based on all tree-level graphs contributing to the four-fermion final state i . The calculation of matrix elements is done with the EXCALIBUR [18] event generator.

The total accepted signal cross section for a given set of parameters Ψ_{fit} is then:

$$\sigma_i(\Psi_{\text{fit}}) = \frac{\sigma_i^{\text{gen}}}{N_i^{\text{gen}}} \cdot \sum_j R_i(j, \Psi_{\text{fit}}, \Psi_{\text{gen}}), \quad (3)$$

where σ_i^{gen} denotes the cross section corresponding to the total Monte Carlo sample containing N_i^{gen} events. The sum extends over all Monte Carlo events j accepted by the event selection.

Based on the sample of reweighted events, two methods are used to obtain the accepted differential signal cross section in reconstructed invariant mass m_{inv} . Both methods take detector and selection effects as well as Ψ -dependent changes of efficiencies and purities properly into account.

In the box method [32], the accepted differential cross section is determined by averaging Monte Carlo events inside a m_{inv} -bin centred around each data event. The size of the bin considered is limited by the requirement of including no more than 1000 Monte Carlo events, yielding bin sizes of about ± 35 MeV at the peak of the invariant mass distribution. In addition, the bin size must not be larger than ± 250 MeV around m_{inv} .

In the spline method, the continuous function describing the accepted differential cross section is obtained by using a cubic spline to smooth the binned distribution of reconstructed invariant masses. At the kinematic limit of $\sqrt{s}/2$ the value of the spline is fixed to zero, while at the lower bound of 65 GeV the value of the spline is fixed to the average over a 2 GeV interval. The spline contains 25 knots in total. Four knots are placed at each endpoint with the remaining knots placed such that an equal number of Monte Carlo events separates each knot.

Both methods yield identical results within 15% of the statistical error. For the numerical results quoted in the following, the spline method is used.

The fit procedure described above determines the parameters without any bias as long as the Monte Carlo describes photon radiation and detector effects such as resolution and acceptance

functions correctly. By fitting large Monte Carlo samples, typically a hundred times the data, the fitting procedure is tested to high accuracy. The fits reproduce well the values of the parameters of the large Monte Carlo samples being fitted. Also, the fit results do not depend on the values of the parameters Ψ_{gen} of the Monte Carlo sample subject to the reweighting procedure.

The reliability of the errors given by the fit is tested by fitting for each final state several hundred small Monte Carlo samples, each the size of the data samples. The width of the distribution of the fitted central values agrees well with the mean of the distribution of the fitted errors.

5 Mass and Total Width of the W Boson

Based on the data collected at 172 GeV and at 183 GeV, the mass of the W boson is determined for each of the final states $qqe\nu$, $qq\mu\nu$, $qq\tau\nu$ and $qqqq$ in separate maximum likelihood fits. For mass fits in the $qqqq$ channel, the pairing algorithm to assign jets to W bosons used in the event selection [6, 28] is changed. The pairing yielding the highest likelihood in the 5C kinematic fit is chosen. The fraction of correct pairings is reduced to 60% for the best combination and it is 25% for the second best combination. However, the signal-to-background ratio in the relevant signal region around $m_{\text{inv}} \approx 80$ GeV is improved. The loss of correct pairings is recovered by including the pairing with the second highest likelihood as an additional distribution. Monte-Carlo studies show that the two values for M_W obtained from fitting separately the distributions of the best and the second best pairing have a correlation of $(-1.3 \pm 1.0)\%$, which is negligible.

The observed invariant mass distributions together with the fit results for the semileptonic final states are shown in Figure 1. The distributions of the first and second pairing in $qqqq$ events are shown in Figure 2, while the distribution summed over all final states and both $qqqq$ pairings is shown in Figure 3. Combined results are determined by averaging the results of individual channels taking statistical and systematic errors into account. The results of fits for M_W are summarised in Table 1. The observed statistical errors agree well with the statistical errors expected for the size of the data samples used. The results of fits for M_W and Γ_W are summarised in Table 2.

6 Systematic Effects

The systematic errors on the fitted W mass and width are summarised in Tables 3 and 4. They arise from various sources and are divided into systematic errors correlated between final states and systematic errors uncorrelated between final states.

6.1 Correlated Errors

The beam energy of LEP is known with an accuracy of 25 MeV for the 1997 data and 30 MeV for the 1996 data, where 25 MeV of these errors are fully correlated [15]. The relative error on M_W is given by the relative error on the LEP beam energy, while the width is less affected. The spread in centre-of-mass energy of about 0.2 GeV adds in quadrature to detector resolution and total width of the W boson and is thus negligible.

Systematic uncertainties due to incomplete simulations of initial-state radiation (ISR) are estimated by comparing the Monte Carlo generators KORALW and EXCALIBUR implementing

different QED radiation schemes. For final-state radiation (FSR), events with FSR simulation are compared to events without any FSR and a third of the difference is taken as a systematic error.

The reconstruction of hadronic jets is examined by studying hadronic $q\bar{q}(\gamma)$ events collected at the Z pole and at 183 GeV. A systematic error for the jet measurement is assigned from varying the jet energy scale by 0.2 GeV, smearing the jet energies by 5% and smearing the jet positions by 0.5° . Effects due to fragmentation and particle decays are determined by comparing signal events simulated using string fragmentation as implemented in the PYTHIA Monte Carlo program and cluster fragmentation as implemented in the HERWIG Monte Carlo program to simulate the hadronisation process.

The fitting method itself is tested by fitting to various Monte Carlo samples generated with known values for M_W and Γ_W , varying over a range of ± 0.5 GeV. The systematic error due to the fitting method includes the effects due to different procedures for reweighting and smoothing of the invariant mass distributions and choice of technical parameters such as spline parameters, box size and occupancy.

Limited Monte Carlo statistics introduces a tendency of the method to have a slope of the linear function relating fitted mass to generated mass less than one. All Monte Carlo samples, approximately one million events, are used in the reweighting procedure to minimise this effect when fitting data. Fitting several Monte Carlo samples and using the remaining Monte Carlo as reference the non-linearity is found to be negligible.

6.2 Uncorrelated Errors

The systematic error due to the size of the signal Monte Carlo sample used for reweighting is estimated by dividing it into N parts of equal size, N between 2 and 100, and making N fits to the same data sample. The spread of the fit results, divided by the square root of N-1, is found to be independent of N and yields the systematic error due to Monte Carlo statistics.

Selection effects are estimated by varying the cut on the probability of the kinematic fit and the interval of reconstructed invariant masses being fitted. Effects due to background are determined by varying both the total accepted background cross section within its error as evaluated for the cross section measurement as well as the shape of the invariant mass spectrum arising from the background.

For $qqqq$ events, strong final state interactions (FSI) between the hadronic systems of the two decaying W bosons due to effects of colour-reconnection [33, 34] or Bose-Einstein correlations [35, 36] may affect the mass reconstruction. In both cases, possible effects are estimated by comparing signal simulations including and excluding the modelling of such effects and assigning the mass difference found as systematic error. In case of colour reconnection, two models, called superconductor model type I and type II as implemented in PYTHIA 5.7 are studied [34], adjusted such that they both yield 35% reconnection probability. In case of Bose-Einstein correlations, the simulation of this effect as implemented in PYTHIA 5.7 is used [36].

For $qqe\nu$ and $qq\mu\nu$ events, the reconstruction of the lepton energy and angles also affects the invariant mass reconstruction. In analogy to hadronic jets, control samples of $\ell^+\ell^-(\gamma)$ events selected at the Z pole are used to cross check the reconstruction of leptons. Energy scales and resolutions are varied within their errors and the resulting effect on W mass and width is quoted as a systematic error.

6.3 Z Mass Reconstruction as Consistency Check

All aspects of the mass measurement, ranging from detector calibration and jet reconstruction to fitting method are checked using $e^+e^- \rightarrow q\bar{q}\gamma$ events selected at $\sqrt{s} = 183$ GeV. For such events, the hard initial-state radiative photon reduces the centre-of-mass energy of the e^+e^- interaction. The presence of the Z resonance causes the distribution of the invariant mass of the jet-jet system to exhibit a peak at the Z mass, as it originates from Z decay, with a shape similar to the W mass spectrum.

A kinematic fit is used to improve the mass resolution, enforcing four-momentum conservation in order to improve resolutions in energies and angles of measured photons and of the two jets and to determine the energy of one photon or two photons escaping along the beam axis. For the extraction of the Z mass from the invariant mass spectrum the same method as for the W mass measurement is applied. Monte Carlo events are reweighted according to the ratio:

$$R_Z(\sqrt{s'}, M_{\text{fit}}^Z, M_{\text{gen}}^Z) = \frac{\frac{d\sigma}{d\sqrt{s'}}(\sqrt{s'}, M_{\text{fit}}^Z)}{\frac{d\sigma}{d\sqrt{s'}}(\sqrt{s'}, M_{\text{gen}}^Z)}, \quad (4)$$

using the differential cross-section $d\sigma/d\sqrt{s'}$ where $\sqrt{s'}$ is the reduced centre-of-mass energy after initial-state radiation at Monte Carlo generator level.

The reconstructed mass spectrum together with the fit result is shown in Figure 4. A total of 3351 events are selected in a mass window ranging from 70 GeV to 110 GeV. The fitted Z-mass value is $M_Z = 91.172 \pm 0.098$ GeV, where the error is statistical. Within this error, the fitted Z mass agrees well with our measurement of the Z mass derived from cross section measurements at centre-of-mass energies close to the Z pole, $M_Z = 91.195 \pm 0.009$ GeV [37]. The good agreement represents an important test of the complete mass analysis method.

7 Results

The results on M_W determined in the $qqe\nu$, $qq\mu\nu$, and $qq\tau\nu$ final states are in good agreement with each other, as shown in Table 1. They are averaged taking statistical and systematic errors including correlations into account, and compared to the result on M_W determined in the $qqqq$ final state, also shown in Table 1. The systematic error on the mass derived from $qqqq$ events contains a contribution from possible strong FSI effects. Within the statistical accuracy of these measurements there is no significant difference between M_W as determined in $qq\ell\nu$ and $qqqq$ events:

$$\Delta M_W = M_W(qqqq) - M_W(qq\ell\nu) = 0.35 \pm 0.28 \text{ (stat.)} \pm 0.05 \text{ (syst.) GeV}. \quad (5)$$

For the calculation of the systematic error on the mass difference, the systematic errors due to strong FSI are not included.

Averaging the results on M_W obtained from the $qq\ell\nu$ and $qqqq$ event samples, including also FSI errors, yields:

$$M_W = 80.58 \pm 0.14 \text{ (stat.)} \pm 0.08 \text{ (syst.) GeV}. \quad (6)$$

The summed mass distribution is shown in Figure 3 and compared to the expectation based on this W-mass value. The good agreement between the data and the reweighted mass spectrum is quantified by the χ^2 value of 26 for 30 degrees of freedom which corresponds to a probability

of 66%. The mass values obtained in fits which determine both M_W and Γ_W are the same as before within 20 MeV while the error on the mass is unchanged.

Within the statistical error, the width of the W boson determined in $qqqq$ and $qq\ell\nu$ events agree as shown in Table 2. For all final states combined the result is:

$$\Gamma_W = 1.97 \pm 0.34 \text{ (stat.)} \pm 0.17 \text{ (syst.) GeV}, \quad (7)$$

with a correlation coefficient of +10% between M_W and Γ_W as shown in Figure 5. Our result on Γ_W is in good agreement with the indirect measurement at $p\bar{p}$ colliders, 2.07 ± 0.06 GeV [4], and measurements at LEP [13, 38]. It also agrees well with the Standard Model expectation, 2.08 GeV, calculated for the current world-average W mass [39].

The results on M_W presented here agree well with our result derived from the measurements of the total W-pair production cross section, $M_W = 80.78^{+0.45}_{-0.41}$ (*exp.*) ± 0.03 (LEP) GeV [6]. Combining both results yields:

$$M_W = 80.61 \pm 0.15 \text{ GeV}. \quad (8)$$

This direct determination of M_W is in good agreement with the direct determination of M_W at $p\bar{p}$ colliders [3] and at LEP at lower centre-of-mass energies [7–9, 11–13] and at 183 GeV [38]. It also agrees with our indirect determination of M_W at the Z peak, $M_W = 80.22 \pm 0.22$ GeV [37], testing the Standard Model at the level of its electroweak corrections.

8 Acknowledgements

We wish to congratulate the CERN accelerator divisions for the successful upgrade of the LEP machine and to express our gratitude for its good performance. We acknowledge with appreciation the effort of the engineers, technicians and support staff who have participated in the construction and maintenance of this experiment.

References

- [1] S. L. Glashow, Nucl. Phys. **22** (1961) 579;
S. Weinberg, Phys. Rev. Lett. **19** (1967) 1264;
A. Salam, in *Elementary Particle Theory*, ed. N. Svartholm, Stockholm, Almqvist and Wiksell (1968), 367.
- [2] Z. Kunszt *et al.*, in *Physics at LEP 2*, Report CERN 96-01 (1996), eds G. Altarelli, T. Sjöstrand, F. Zwirner, Vol. 1, p. 141.
- [3] The UA1 Collaboration, C. Albajar *et al.*, Z. Phys. **C 44** (1989) 15;
The UA2 Collaboration, J. Alitti *et al.*, Phys. Lett. **B 241** (1990) 150; Phys. Lett. **B 276** (1992) 354;
The CDF Collaboration, F. Abe *et al.*, Phys. Rev. Lett. **65** (1990) 2243; Phys. Rev. **D 43** (1991) 2070; Phys. Rev. Lett. **75** (1995) 11; Phys. Rev. **D 52** (1995) 4784;
The DØ Collaboration, S. Abachi *et al.*, Phys. Rev. Lett. **77** (1996) 3309; B. Abbott *et al.*, Phys. Rev. **D 58** (1998) 012002; B. Abbott *et al.*, Phys. Rev. Lett. **80** (1998) 3008; B. Abbott *et al.*, Phys. Rev. **D 58** (1998) 092003.
- [4] The UA1 Collaboration, C. Albajar *et al.*, Phys. Lett. **B 253** (1991) 503;
The UA2 Collaboration, J. Alitti *et al.*, Phys. Lett. **B 276** (1992) 365;
The CDF Collaboration, F. Abe *et al.*, Phys. Rev. Lett. **74** (1995) 341; Phys. Rev. **D 52** (1995) 2624;
The DØ Collaboration, S. Abachi *et al.*, Phys. Rev. Lett. **75** (1995) 1456.
- [5] The L3 Collaboration, M. Acciarri *et al.*, Phys. Lett. **B 398** (1997) 223.
- [6] The L3 Collaboration, M. Acciarri *et al.*, Phys. Lett. **B 407** (1997) 419.
- [7] The ALEPH Collaboration, R. Barate *et al.*, Phys. Lett. **B 401** (1997) 347.
- [8] The DELPHI Collaboration, P. Abreu *et al.*, Phys. Lett. **B 397** (1997) 158.
- [9] The OPAL Collaboration, K. Ackerstaff *et al.*, Phys. Lett. **B 389** (1996) 416.
- [10] The L3 Collaboration, M. Acciarri *et al.*, Phys. Lett. **B 413** (1997) 176.
- [11] The ALEPH Collaboration, R. Barate *et al.*, Phys. Lett. **B 422** (1998) 384.
- [12] The DELPHI Collaboration, P. Abreu *et al.*, Euro. Phys. Jour. **C 2** (1998) 581.
- [13] The OPAL Collaboration, K. Ackerstaff *et al.*, Euro. Phys. Jour. **C 1** (1998) 425.
- [14] The L3 Collaboration, B. Adeva *et al.*, Nucl. Instr. and Meth. **A 289** (1990) 35;
M. Chemarin *et al.*, Nucl. Instr. and Meth. **A 349** (1994) 345;
M. Acciarri *et al.*, Nucl. Instr. and Meth. **A 351** (1994) 300;
G. Basti *et al.*, Nucl. Instr. and Meth. **A 374** (1996) 293;
I.C. Brock *et al.*, Nucl. Instr. and Meth. **A 381** (1996) 236;
A. Adam *et al.*, Nucl. Instr. and Meth. **A 383** (1996) 342.
- [15] The LEP Energy Working Group, *Evaluation of the LEP centre-of-mass energy above W-pair production threshold*, CERN-EP/98-191.

- [16] KORALW version 1.33 is used.
M. Skrzypek, S. Jadach, W. Placzek and Z. Wąs, *Comp. Phys. Comm.* **94** (1996) 216;
M. Skrzypek, S. Jadach, M. Martinez, W. Placzek and Z. Wąs, *Phys. Lett.* **B 372** (1996) 289.
- [17] HERWIG version 5.9 is used.
G. Marchesini and B. Webber, *Nucl. Phys.* **B 310** (1988) 461;
I.G. Knowles, *Nucl. Phys.* **B 310** (1988) 571;
G. Marchesini *et al.*, *Comp. Phys. Comm.* **67** (1992) 465.
- [18] F.A. Berends, R. Kleiss and R. Pittau, *Nucl. Phys.* **B 424** (1994) 308; *Nucl. Phys.* **B 426** (1994) 344; *Nucl. Phys. (Proc. Suppl.)* **B 37** (1994) 163;
R. Kleiss and R. Pittau, *Comp. Phys. Comm.* **83** (1994) 141;
R. Pittau, *Phys. Lett.* **B 335** (1994) 490.
- [19] PYTHIA version 5.722 is used.
T. Sjöstrand, *PYTHIA 5.7 and JETSET 7.4 Physics and Manual*,
CERN-TH/7112/93 (1993), revised August 1995; *Comp. Phys. Comm.* **82** (1994) 74.
- [20] KORALZ version 4.02 is used.
S. Jadach, B. F. L. Ward and Z. Wąs, *Comp. Phys. Comm.* **79** (1994) 503.
- [21] J.H. Field, *Phys. Lett.* **B 323** (1994) 432;
J.H. Field and T. Riemann, *Comp. Phys. Comm.* **94** (1996) 53.
- [22] BHWIDE version 1.01 is used.
S. Jadach, W. Placzek, B.F.L. Ward, *Phys. Rev.* **D 40** (1989) 3582, *Comp. Phys. Comm.* **70** (1992) 305, *Phys. Lett.* **B 390** (1997) 298.
- [23] D. Karlen, *Nucl. Phys.* **B 289** (1987) 23.
- [24] F. A. Berends, P. H. Daverfeldt and R. Kleiss, *Nucl. Phys.* **B 253** (1985) 441.
- [25] J.A.M. Vermaseren, J. Smith and G. Grammer Jr, *Phys. Rev.* **D 19** (1979) 137;
J.A.M. Vermaseren, *Nucl. Phys.* **B 229** (1983) 347.
- [26] PHOJET version 1.05 is used.
R. Engel, *Z. Phys.* **C 66** (1995) 203; R. Engel and J. Ranft, *Phys. Rev.* **D 54** (1996) 4244.
- [27] The L3 detector simulation is based on GEANT Version 3.15.
R. Brun *et al.*, *GEANT 3*, CERN-DD/EE/84-1 (Revised), 1987.
The GHEISHA program (H. Fesefeldt, RWTH Aachen Report PITHA 85/02 (1985))
is used to simulate hadronic interactions.
- [28] The L3 Collaboration, M. Acciarri *et al.*, *Phys. Lett.* **B 436** (1998) 437.
- [29] W. Beenakker *et al.*, in *Physics at LEP 2*, Report CERN 96-01 (1996), eds G. Altarelli,
T. Sjöstrand, F. Zwirner, Vol. 1, p. 79.
- [30] D. Bardin *et al.*, *Nucl. Phys. (Proc. Suppl.)* **B 37** (1994) 148;
F.A. Berends *et al.*, *Nucl. Phys. (Proc. Suppl.)* **B 37** (1994) 163.

- [31] D. Bardin *et al.*, in *Physics at LEP 2*, Report CERN 96-01 (1996), eds G. Altarelli, T. Sjöstrand, F. Zwirner, Vol. 2, p. 3.
- [32] D.M. Schmidt, R.J. Morrison and M.S. Witherell, Nucl. Instr. and Meth. **A 328** (1993) 547.
- [33] G. Gustafson, U. Petterson and P.M. Zerwas, Phys. Lett. **B 209** (1988) 90;
T. Sjöstrand and V.A. Khoze, Z. Phys. **C 62** (1994) 281, Phys. Rev. Lett. **72** (1994) 28;
E. Accomando, A. Ballestrero and E. Maina, Phys. Lett. **B 362** (1995) 141;
G. Gustaffson and J. Häkkinen, Z. Phys. **C 64** (1994) 659;
L. Lönnblad, Z. Phys. **C 70** (1996) 107;
J. Ellis and K. Geiger, Phys. Rev. **D 54** (1996) 1967, Phys. Lett. **B 404** (1997) 230.
- [34] T. Sjöstrand and V.A. Khoze, Z. Phys. **C 62** (1994) 281.
- [35] S. Jadach and K. Zalewski, Acta Phys. Polon **B 28** (1997) 1363.
- [36] L. Lönnblad and T. Sjöstrand, Phys. Lett. **B 351** (1995) 293.
- [37] The L3 Collaboration, M. Acciarri *et al.*, Z. Phys. **C 62** (1994) 551.
- [38] The OPAL Collaboration, G. Abbiendi *et al.*, CERN-EP/98-197.
- [39] C. Caso *et al.*, *The 1998 Review of Particle Physics*, Euro. Phys. Jour. **C 3** (1998) 1.

The L3 Collaboration:

M. Acciari,²⁶ P. Achard,¹⁸ O. Adriani,¹⁵ M. Aguilar-Benitez,²⁵ J. Alcaraz,²⁵ G. Alemanni,²¹ J. Allaby,¹⁶ A. Aloisio,²⁸ M. G. Alvigi,²⁸ G. Ambrosi,¹⁸ H. Anderhub,⁴⁷ V. P. Andreev,^{6,36} T. Angelescu,¹² F. Anselmo,⁹ A. Arefiev,²⁷ T. Azemoon,³ T. Aziz,¹⁰ P. Bagnaia,³⁵ L. Baksay,⁴² A. Balandras,⁴ R. C. Ball,³ S. Banerjee,¹⁰ Sw. Banerjee,¹⁰ K. Banicz,⁴⁴ A. Barczyk,^{47,45} R. Barillere,¹⁶ L. Barone,³⁵ P. Bartalini,²¹ M. Basile,⁹ R. Battiston,³² A. Bay,²¹ F. Becattini,¹⁵ U. Becker,¹⁴ F. Behner,⁴⁷ J. Berdugo,²⁵ P. Berges,¹⁴ B. Bertucci,³² B. L. Betev,⁴⁷ S. Bhattacharya,¹⁰ M. Biasini,³² A. Biland,⁴⁷ J. J. Blaising,⁴ S. C. Blyth,³³ G. J. Bobbink,² A. Böhm,¹ L. Boldizsar,¹³ B. Borgia,^{16,35} D. Bourilkov,⁴⁷ M. Bourquin,¹⁸ S. Braccini,¹⁸ J. G. Branson,³⁸ V. Brigljevic,⁴⁷ F. Brochu,⁴ A. Buffini,¹⁵ A. Buijs,⁴³ J. D. Burger,¹⁴ W. J. Burger,³² J. Busenitz,⁴² A. Button,³ X. D. Cai,¹⁴ M. Campanelli,⁴⁷ M. Capell,¹⁴ G. Cara Romeo,⁹ G. Carlino,²⁸ A. M. Cartacci,¹⁵ J. Casaus,²⁵ G. Castellini,¹⁵ F. Cavallari,³⁵ N. Cavallo,²⁸ C. Cecchi,¹⁸ M. Cerrada,²⁵ F. Cesaroni,²² M. Chamizo,¹⁸ Y. H. Chang,⁴⁹ U. K. Chaturvedi,¹⁷ M. Chemarin,²⁴ A. Chen,⁴⁹ G. Chen,⁷ G. M. Chen,⁷ H. F. Chen,¹⁹ H. S. Chen,⁷ X. Chereau,⁴ G. Chiefari,²⁸ L. Cifarelli,³⁷ F. Cindolo,⁹ C. Civinini,¹⁵ I. Clare,¹⁴ R. Clare,¹⁴ G. Coignet,⁴ A. P. Colijn,² N. Colino,²⁵ S. Costantini,⁸ F. Cotorobai,¹² B. Cozzoni,⁹ B. de la Cruz,²⁵ A. Csilling,¹³ T. S. Dai,¹⁴ J. A. van Dalen,³⁰ R. D' Alessandro,¹⁵ R. de Asmundis,²⁸ P. Deglon,¹⁸ A. Degré,⁴ K. Deiters,⁴⁵ D. della Volpe,²⁸ P. Denes,³⁴ F. DeNotaristefani,³⁵ A. De Salvo,⁴⁷ M. Diemoz,³⁵ D. van Dierendonck,² F. Di Lodovico,⁴⁷ C. Dionisi,^{16,35} M. Dittmar,⁴⁷ A. Dominguez,³⁸ A. Doria,²⁸ M. T. Dova,^{17,‡} D. Duchesneau,⁴ D. Dufournand,⁴ P. Duinker,² I. Duran,³⁹ H. El Mamouni,²⁴ A. Engler,³³ F. J. Eppling,¹⁴ F. C. Erné,² P. Extermann,¹⁸ M. Fabre,⁴⁵ R. Faccini,³⁵ M. A. Falagan,²⁵ S. Falciano,³⁵ A. Favara,¹⁵ J. Fay,²⁴ O. Fedin,³⁶ M. Felcini,⁴⁷ T. Ferguson,³³ F. Ferroni,³⁵ H. Fesefeldt,¹ E. Fiandrini,³² J. H. Field,¹⁸ F. Filthaut,¹⁶ P. H. Fisher,¹⁴ I. Fisk,³⁸ G. Forconi,¹⁴ L. Fredj,¹⁸ K. Freudenreich,⁴⁷ C. Furetta,²⁶ Yu. Galaktionov,^{27,14} S. N. Ganguli,¹⁰ P. Garcia-Abia,⁵ M. Gataullin,³¹ S. S. Gau,¹¹ S. Gentile,³⁵ N. Gheordanescu,¹² S. Giagu,³⁵ Z. F. Gong,¹⁹ G. Grenier,²⁴ M. W. Gruenewald,⁸ R. van Gulik,² V. K. Gupta,³⁴ A. Gurtu,¹⁰ L. J. Gutay,⁴⁴ D. Haas,⁵ A. Hasan,²⁹ D. Hatzifotiadou,⁹ T. Hebbeker,⁸ A. Hervé,¹⁶ P. Hidas,¹³ J. Hirschfelder,³³ H. Hofer,⁴⁷ G. Holzner,⁴⁷ H. Hoorani,³³ S. R. Hou,⁴⁹ I. Iashvili,⁴⁶ B. N. Jin,⁷ L. W. Jones,³ P. de Jong,² I. Josa-Mutuberría,²⁵ R. A. Khan,¹⁷ D. Kamrad,⁴⁶ J. S. Kapustinsky,²³ M. Kaur,^{17,‡} M. N. Kienzle-Focacci,¹⁸ D. Kim,³⁵ D. H. Kim,⁴¹ J. K. Kim,⁴¹ S. C. Kim,⁴¹ W. W. Kinnison,²³ J. Kirkby,¹⁶ D. Kiss,¹³ W. Kittel,³⁰ A. Klimentov,^{14,27} A. C. König,³⁰ A. Kopp,⁴⁶ I. Korolko,²⁷ V. Koutsenko,^{14,27} R. W. Kraemer,³³ W. Krenz,¹ A. Kunin,^{14,27} P. Lacentre,^{46,‡,‡} P. Ladron de Guevara,²⁵ I. Laktineh,²⁴ G. Landi,¹⁵ K. Lassila-Perini,⁴⁷ P. Laurikainen,²⁰ A. Lavorato,³⁷ M. Lebeau,¹⁶ A. Lebedev,¹⁴ P. Lebrun,²⁴ P. Lecomte,⁴⁷ P. Lecoq,¹⁶ P. Le Coultre,⁴⁷ H. J. Lee,⁸ J. M. Le Goff,¹⁶ R. Leiste,⁴⁶ E. Leonardi,³⁵ P. Levchenko,³⁶ C. Li,¹⁹ C. H. Lin,⁴⁹ W. T. Lin,⁴⁹ F. L. Linde,^{2,16} L. Lista,²⁸ Z. A. Liu,⁷ W. Lohmann,⁴⁶ E. Longo,³⁵ Y. S. Lu,⁷ K. Lübelmeyer,¹ C. Luci,^{16,35} D. Luckey,¹⁴ L. Lugnier,²⁴ L. Luminari,³⁵ W. Lustermaier,⁴⁷ W. G. Ma,¹⁹ M. Maity,¹⁰ G. Majumder,¹⁰ L. Malgeri,¹⁶ A. Malinin,²⁷ C. Mañá,²⁵ D. Mangeol,³⁰ P. Marchesini,⁴⁷ G. Marian,^{42,¶} J. P. Martin,²⁴ F. Marzano,³⁵ G. G. G. Massaro,² K. Mazumdar,¹⁰ R. R. McNeil,⁶ S. Mele,¹⁶ L. Merola,²⁸ M. Meschini,¹⁵ W. J. Metzger,³⁰ M. von der Mey,¹ D. Miganí,⁹ A. Mihul,¹² H. Milcent,¹⁶ G. Mirabelli,³⁵ J. Mnich,¹⁶ P. Molnar,⁸ B. Monteleoni,¹⁵ T. Moulík,¹⁰ G. S. Muanza,²⁴ F. Muheim,¹⁸ A. J. M. Muijers,²⁸ M. Napolitano,²⁸ F. Nessi-Tedaldi,⁴⁷ H. Newman,³¹ T. Niessen,¹ A. Nisati,³⁵ H. Nowak,⁴⁶ Y. D. Oh,⁴¹ G. Organtini,³⁵ R. Ostonen,²⁰ C. Palomares,²⁵ D. Pandoulas,¹ S. Paoletti,^{35,16} P. Paolucci,²⁸ H. K. Park,³³ I. H. Park,⁴¹ G. Pascale,³⁵ G. Passaleva,¹⁶ S. Patricelli,²⁸ T. Paul,¹¹ M. Pauluzzi,³² C. Paus,¹⁶ F. Pauss,⁴⁷ D. Peach,¹⁶ M. Pedace,³⁵ Y. J. Pei,¹ S. Pensotti,²⁶ D. Perret-Gallix,⁴ B. Petersen,³⁰ S. Petrak,⁸ D. Piccolo,²⁸ M. Pieri,¹⁵ P. A. Piroué,³⁴ E. Pistolesi,²⁶ V. Plyaskin,²⁷ M. Pohl,⁴⁷ V. Pojidaev,^{27,15} H. Postema,¹⁴ J. Pothier,¹⁶ N. Produit,¹⁸ D. Prokofiev,³⁶ J. Quartieri,³⁷ G. Rahal-Callot,⁴⁷ N. Raja,¹⁰ P. G. Rancoita,²⁶ G. Raven,³⁸ P. Razi,²⁹ D. Ren,⁴⁷ M. Rescigno,³⁵ S. Reucroft,¹¹ T. van Rhee,⁴³ S. Riemann,⁴⁶ K. Riles,³ A. Robohm,⁴⁷ J. Rodin,⁴² B. P. Roe,³ L. Romero,²⁵ S. Rosier-Lees,⁴ J. A. Rubio,¹⁶ D. Ruschmeier,⁸ H. Rykaczewski,⁴⁷ S. Sakar,³⁵ J. Salicio,¹⁶ E. Sanchez,¹⁶ M. P. Sanders,³⁰ M. E. Sarakinos,²⁰ C. Schäfer,¹ V. Schegelsky,³⁶ S. Schmidt-Kaerst,¹ D. Schmitz,¹ N. Scholz,⁴⁷ H. Schopper,⁴⁸ D. J. Schotanus,³⁰ J. Schwenke,¹ G. Schwering,¹ C. Sciacca,²⁸ D. Sciarrino,¹⁸ A. Seganti,⁹ L. Servoli,³² S. Shevchenko,³¹ N. Shivarov,⁴⁰ V. Shoutko,²⁷ J. Shukla,²³ E. Shumilov,²⁷ A. Shvorob,³¹ T. Siedenburger,¹ D. Son,⁴¹ B. Smith,³³ P. Spillantini,¹⁵ M. Steuer,¹⁴ D. P. Stickland,³⁴ A. Stone,⁶ H. Stone,³⁴ B. Stoyanov,⁴⁰ A. Straessner,¹ K. Sudhakar,¹⁰ G. Sultanov,¹⁷ L. Z. Sun,¹⁹ H. Suter,⁴⁷ J. D. Swain,¹⁷ Z. Szillasi,^{42,¶} X. W. Tang,⁷ L. Tauscher,⁵ L. Taylor,¹¹ C. Timmermans,³⁰ Samuel C. C. Ting,¹⁴ S. M. Ting,¹⁴ S. C. Tonwar,¹⁰ J. Tóth,¹³ C. Tully,³⁴ K. L. Tung,⁷ Y. Uchida,¹⁴ J. Ulbricht,⁴⁷ E. Valente,³⁵ G. Vesztegombi,¹³ I. Vetlitsky,²⁷ D. Vicinanza,³⁷ G. Viertel,⁴⁷ S. Villa,¹¹ M. Vivargent,⁴ S. Vlachos,⁵ I. Vodopianov,³⁶ H. Vogel,³³ H. Vogt,⁴⁶ I. Vorobiev,^{16,27} A. A. Vorobyov,³⁶ A. Vorvolakos,²⁹ M. Wadhwa,⁵ W. Wallraff,¹ M. Wang,¹⁴ X. L. Wang,¹⁹ Z. M. Wang,¹⁹ A. Weber,¹ M. Weber,¹ P. Wienemann,¹ H. Wilkens,³⁰ S. X. Wu,¹⁴ S. Wynhoff,¹ L. Xia,³¹ Z. Z. Xu,¹⁹ B. Z. Yang,¹⁹ C. G. Yang,⁷ H. J. Yang,⁷ M. Yang,⁷ J. B. Ye,¹⁹ S. C. Yeh,⁵⁰ J. M. You,³³ An. Zalite,³⁶ Yu. Zalite,³⁶ P. Zemp,⁴⁷ Z. P. Zhang,¹⁹ G. Y. Zhu,⁷ R. Y. Zhu,³¹ A. Zichichi,^{9,16,17} F. Ziegler,⁴⁶ G. Zilizi,^{42,¶} M. Zöller,¹

- 1 I. Physikalisches Institut, RWTH, D-52056 Aachen, FRG[§]
 - III. Physikalisches Institut, RWTH, D-52056 Aachen, FRG[§]
 - 2 National Institute for High Energy Physics, NIKHEF, and University of Amsterdam, NL-1009 DB Amsterdam, The Netherlands
 - 3 University of Michigan, Ann Arbor, MI 48109, USA
 - 4 Laboratoire d'Annecy-le-Vieux de Physique des Particules, LAPP, IN2P3-CNRS, BP 110, F-74941 Annecy-le-Vieux CEDEX, France
 - 5 Institute of Physics, University of Basel, CH-4056 Basel, Switzerland
 - 6 Louisiana State University, Baton Rouge, LA 70803, USA
 - 7 Institute of High Energy Physics, IHEP, 100039 Beijing, China[△]
 - 8 Humboldt University, D-10099 Berlin, FRG[§]
 - 9 University of Bologna and INFN-Sezione di Bologna, I-40126 Bologna, Italy
 - 10 Tata Institute of Fundamental Research, Bombay 400 005, India
 - 11 Northeastern University, Boston, MA 02115, USA
 - 12 Institute of Atomic Physics and University of Bucharest, R-76900 Bucharest, Romania
 - 13 Central Research Institute for Physics of the Hungarian Academy of Sciences, H-1525 Budapest 114, Hungary[‡]
 - 14 Massachusetts Institute of Technology, Cambridge, MA 02139, USA
 - 15 INFN Sezione di Firenze and University of Florence, I-50125 Florence, Italy
 - 16 European Laboratory for Particle Physics, CERN, CH-1211 Geneva 23, Switzerland
 - 17 World Laboratory, FBLJA Project, CH-1211 Geneva 23, Switzerland
 - 18 University of Geneva, CH-1211 Geneva 4, Switzerland
 - 19 Chinese University of Science and Technology, USTC, Hefei, Anhui 230 029, China[△]
 - 20 SEFT, Research Institute for High Energy Physics, P.O. Box 9, SF-00014 Helsinki, Finland
 - 21 University of Lausanne, CH-1015 Lausanne, Switzerland
 - 22 INFN-Sezione di Lecce and Università Degli Studi di Lecce, I-73100 Lecce, Italy
 - 23 Los Alamos National Laboratory, Los Alamos, NM 87544, USA
 - 24 Institut de Physique Nucléaire de Lyon, IN2P3-CNRS, Université Claude Bernard, F-69622 Villeurbanne, France
 - 25 Centro de Investigaciones Energéticas, Medioambientales y Tecnológicas, CIEMAT, E-28040 Madrid, Spain^b
 - 26 INFN-Sezione di Milano, I-20133 Milan, Italy
 - 27 Institute of Theoretical and Experimental Physics, ITEP, Moscow, Russia
 - 28 INFN-Sezione di Napoli and University of Naples, I-80125 Naples, Italy
 - 29 Department of Natural Sciences, University of Cyprus, Nicosia, Cyprus
 - 30 University of Nijmegen and NIKHEF, NL-6525 ED Nijmegen, The Netherlands
 - 31 California Institute of Technology, Pasadena, CA 91125, USA
 - 32 INFN-Sezione di Perugia and Università Degli Studi di Perugia, I-06100 Perugia, Italy
 - 33 Carnegie Mellon University, Pittsburgh, PA 15213, USA
 - 34 Princeton University, Princeton, NJ 08544, USA
 - 35 INFN-Sezione di Roma and University of Rome, "La Sapienza", I-00185 Rome, Italy
 - 36 Nuclear Physics Institute, St. Petersburg, Russia
 - 37 University and INFN, Salerno, I-84100 Salerno, Italy
 - 38 University of California, San Diego, CA 92093, USA
 - 39 Dept. de Física de Partículas Elementales, Univ. de Santiago, E-15706 Santiago de Compostela, Spain
 - 40 Bulgarian Academy of Sciences, Central Lab. of Mechatronics and Instrumentation, BU-1113 Sofia, Bulgaria
 - 41 Center for High Energy Physics, Adv. Inst. of Sciences and Technology, 305-701 Taejeon, Republic of Korea
 - 42 University of Alabama, Tuscaloosa, AL 35486, USA
 - 43 Utrecht University and NIKHEF, NL-3584 CB Utrecht, The Netherlands
 - 44 Purdue University, West Lafayette, IN 47907, USA
 - 45 Paul Scherrer Institut, PSI, CH-5232 Villigen, Switzerland
 - 46 DESY-Institut für Hochenergiephysik, D-15738 Zeuthen, FRG
 - 47 Eidgenössische Technische Hochschule, ETH Zürich, CH-8093 Zürich, Switzerland
 - 48 University of Hamburg, D-22761 Hamburg, FRG
 - 49 National Central University, Chung-Li, Taiwan, China
 - 50 Department of Physics, National Tsing Hua University, Taiwan, China
- [§] Supported by the German Bundesministerium für Bildung, Wissenschaft, Forschung und Technologie
[‡] Supported by the Hungarian OTKA fund under contract numbers T019181, F023259 and T024011.
[¶] Also supported by the Hungarian OTKA fund under contract numbers T22238 and T026178.
^b Supported also by the Comisión Interministerial de Ciencia y Tecnología.
[‡] Also supported by CONICET and Universidad Nacional de La Plata, CC 67, 1900 La Plata, Argentina.
[‡] Supported by Deutscher Akademischer Austauschdienst.
[◇] Also supported by Panjab University, Chandigarh-160014, India.
[△] Supported by the National Natural Science Foundation of China.

Process	Events		Mass of the W Boson	Expected Stat.
	172 GeV	183 GeV	M_W [GeV]	Error [GeV]
$e^+e^- \rightarrow qqe\nu(\gamma)$	18	95	$80.21 \pm 0.30 \pm 0.06$	± 0.31
$e^+e^- \rightarrow qq\mu\nu(\gamma)$	9	83	$80.49 \pm 0.36 \pm 0.06$	± 0.34
$e^+e^- \rightarrow qq\tau\nu(\gamma)$	12	75	$80.89 \pm 0.56 \pm 0.08$	± 0.47
$e^+e^- \rightarrow qq\ell\nu(\gamma)$	39	249	$80.41 \pm 0.21 \pm 0.06$	± 0.21
$e^+e^- \rightarrow qqqq(\gamma)$	61	339	$80.75 \pm 0.18 \pm 0.12$	± 0.20
$e^+e^- \rightarrow ffff(\gamma)$	99	588	$80.58 \pm 0.14 \pm 0.08$	± 0.14

Table 1: Number of events used in the analysis and results on the mass of the W boson, M_W , combining the data collected at 172 GeV and at 183 GeV. The first error is statistical and the second systematic. Also shown is the statistical error expected for the size of the data sample analysed.

Process	Mass of the W Boson	Total Decay Width	Correlation
	M_W [GeV]	Γ_W [GeV]	Coefficient
$e^+e^- \rightarrow qq\ell\nu(\gamma)$	$80.42 \pm 0.21 \pm 0.06$	$2.44 \pm 0.59 \pm 0.13$	+0.10
$e^+e^- \rightarrow qqqq(\gamma)$	$80.73 \pm 0.18 \pm 0.12$	$1.69 \pm 0.42 \pm 0.22$	+0.15
$e^+e^- \rightarrow ffff(\gamma)$	$80.58 \pm 0.14 \pm 0.08$	$1.97 \pm 0.34 \pm 0.17$	+0.10

Table 2: Results on the mass of the W boson, M_W , and its total decay width, Γ_W , combining the data collected at 172 GeV and at 183 GeV. The first error is statistical and the second systematic. Also shown is the correlation coefficient between M_W and Γ_W .

Systematic Errors on M_W [MeV]	Final State			
	$qqe\nu$	$qq\mu\nu$	$qq\tau\nu$	$qqqq$
LEP Energy	25	25	25	25
ISR	15	15	15	15
FSR	10	10	10	10
Jet Measurement	30	30	30	5
Fragmentation and Decay	30	30	30	60
Fitting Method	15	15	15	15
Total Correlated	55	55	55	69
MC Statistics	20	20	50	10
Colour Reconnection	—	—	—	70
Bose-Einstein Effects	—	—	—	60
Selection	20	20	20	20
Background	5	10	30	10
Lepton Measurement	15	15	—	—
Total Uncorrelated	32	34	62	95
Total Systematic	63	64	82	118

Table 3: Systematic errors in the determination of M_W for the different final states. The contributions listed in the upper part of the table are treated as correlated when combining different final states. The contributions listed in the lower part are treated as uncorrelated between channels. Total errors are obtained by adding the individual contributions in quadrature.

Systematic Errors on Γ_W [MeV]	Final State	
	$qql\nu$	$qqqq$
LEP Energy	15	15
ISR	25	25
FSR	40	40
Jet Measurement	80	20
Fragmentation and Decay	60	200
Fitting Method	25	25
Total Correlated	114	209
MC Statistics	40	30
Colour Reconnection	—	50
Bose-Einstein Effects	—	10
Selection	40	40
Background	25	25
Lepton Measurement	30	—
Total Uncorrelated	69	76
Total Systematic	133	222

Table 4: Systematic errors in the determination of Γ_W in $qql\nu$ and $qqqq$ production. The contributions listed in the upper part of the table are treated as correlated when combining the two final states. The contributions listed in the lower part are treated as uncorrelated between channels. Total errors are obtained by adding the individual contributions in quadrature.

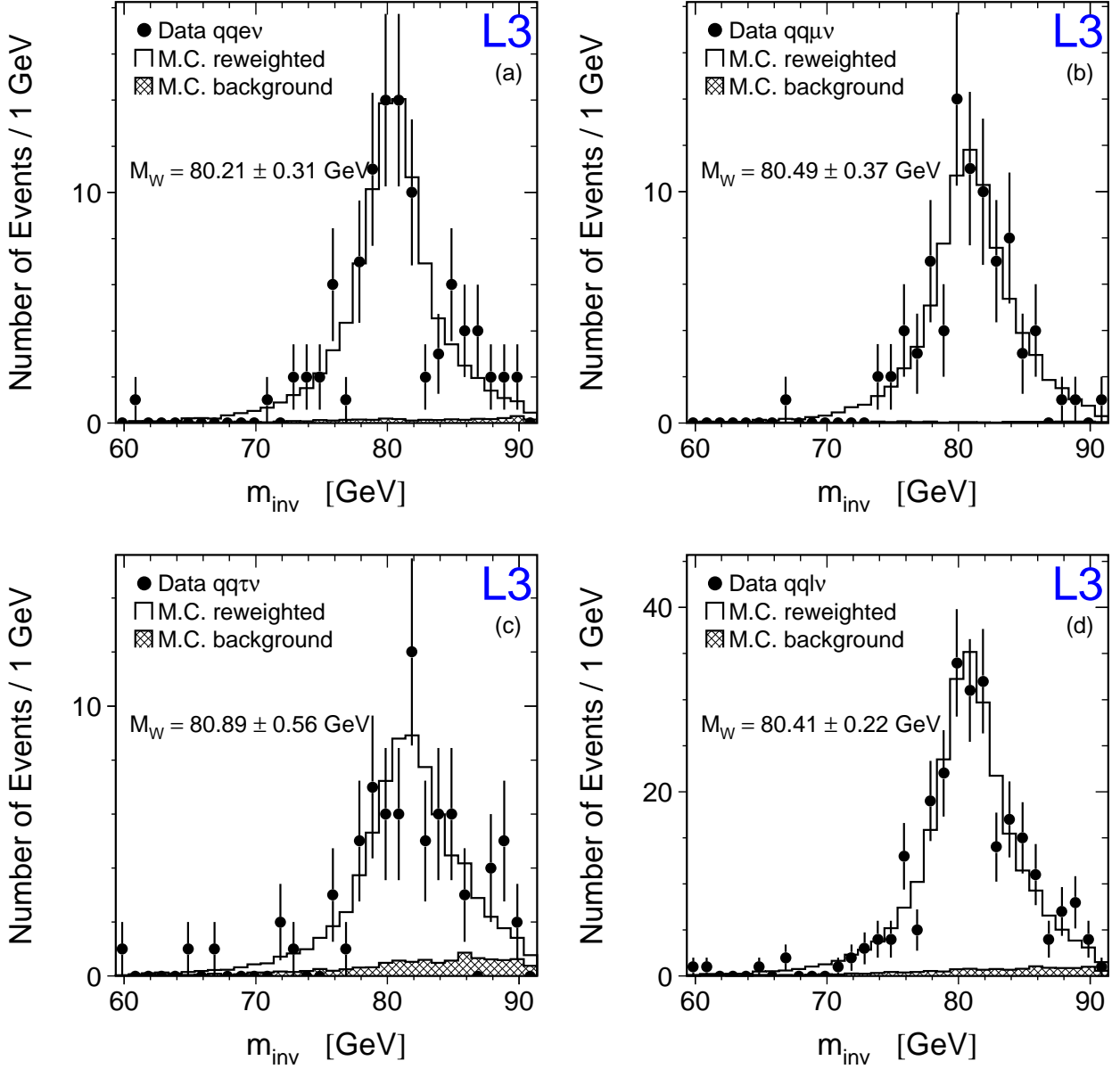


Figure 1: Distributions of reconstructed invariant mass, m_{inv} , after applying the kinematic fit using the equal-mass constraint for events selected in the 183 GeV data: (a) $qqe\nu$, (b) $qq\mu\nu$, (c) $qq\tau\nu$, (d) $qq\ell\nu$, combining $qqe\nu$, $qq\mu\nu$ and $qq\tau\nu$. The solid lines show the result of the fits of M_W to the indicated final states. The quoted error combines statistical and systematic errors in quadrature.

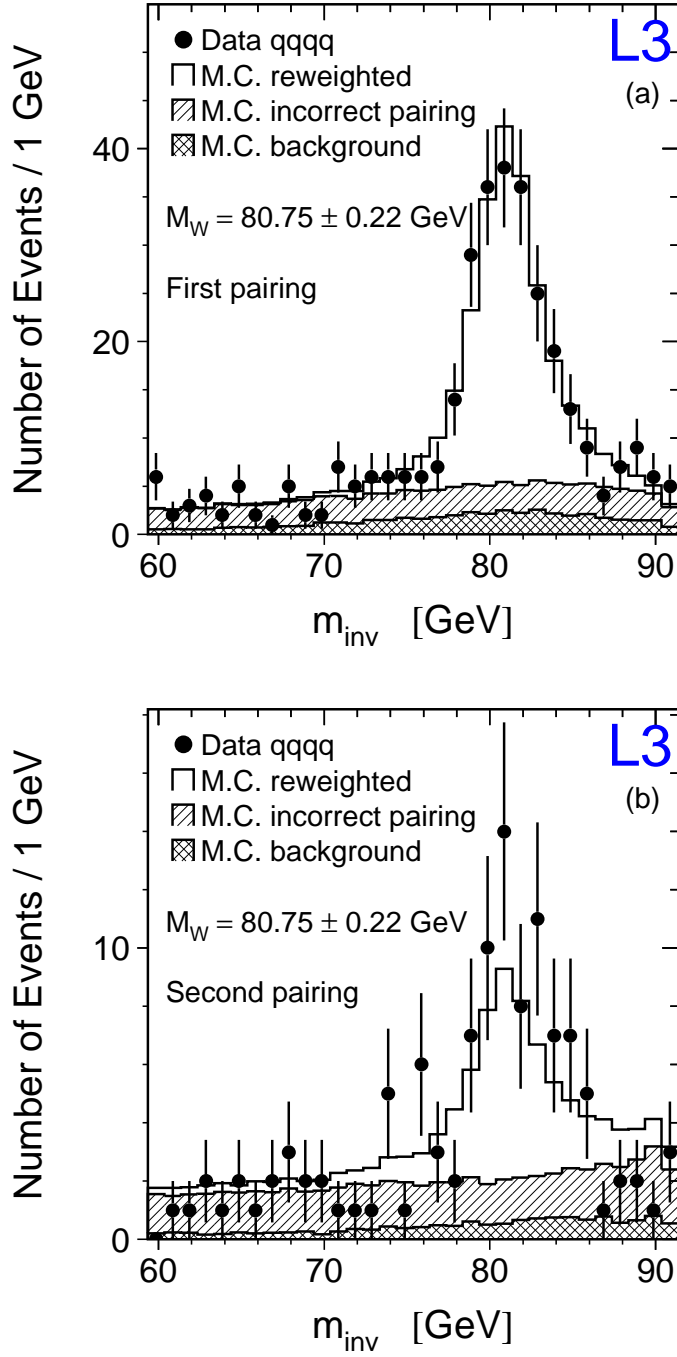


Figure 2: Distributions of reconstructed invariant mass, m_{inv} , after applying the kinematic fit using the equal-mass constraint for $qqqq$ events selected in the 183 GeV data: (a) first pairing, (b) second pairing. The solid lines show the result of the fit of M_W to both pairings. The quoted error combines statistical and systematic errors in quadrature.

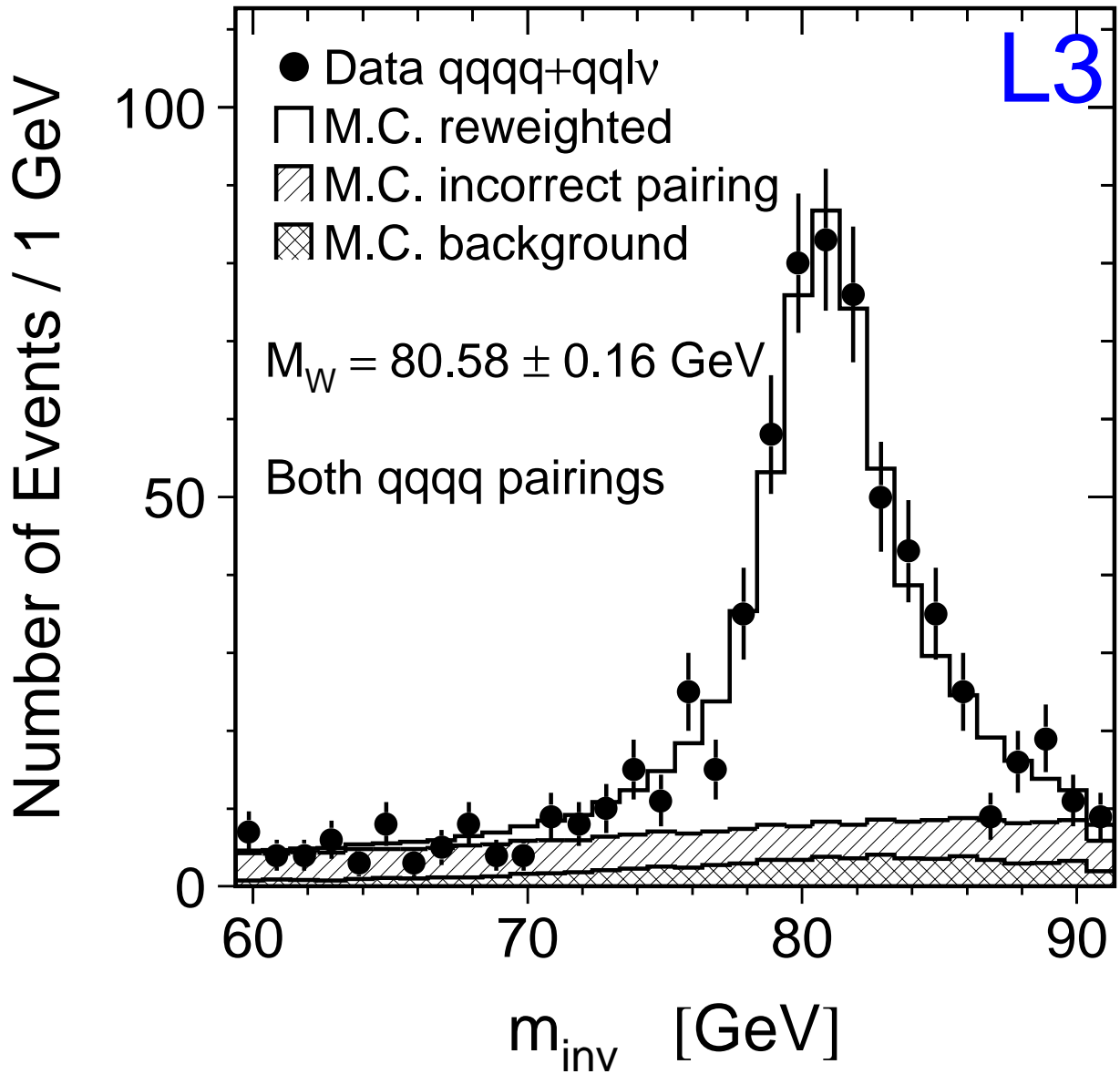


Figure 3: Distribution of reconstructed invariant mass, m_{inv} , after applying the kinematic fit using the equal-mass constraint for all W-pair events selected in the 183 GeV data used for the mass analysis. For $qqqq$ events, both pairings are included. The solid line shows the result of the fit of M_W . The quoted error combines statistical and systematic errors in quadrature.

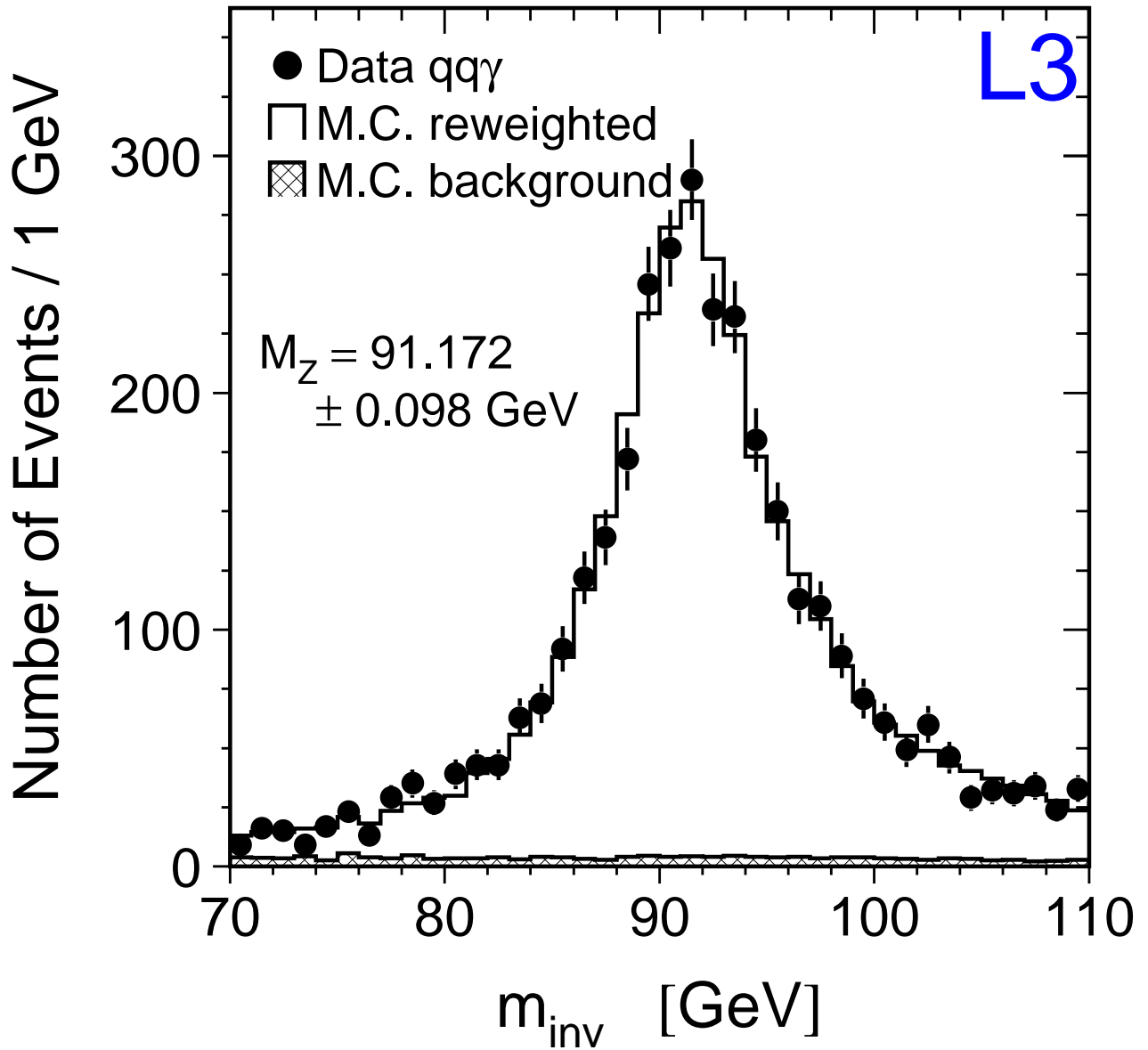


Figure 4: Distribution of reconstructed invariant mass, m_{inv} , after applying the kinematic fit for $q\bar{q}\gamma$ events with hard initial-state radiation selected at 183 GeV. Shown is the region corresponding to the radiative return to the Z. The solid line shows the result of the fit of M_Z . The quoted error is statistical.

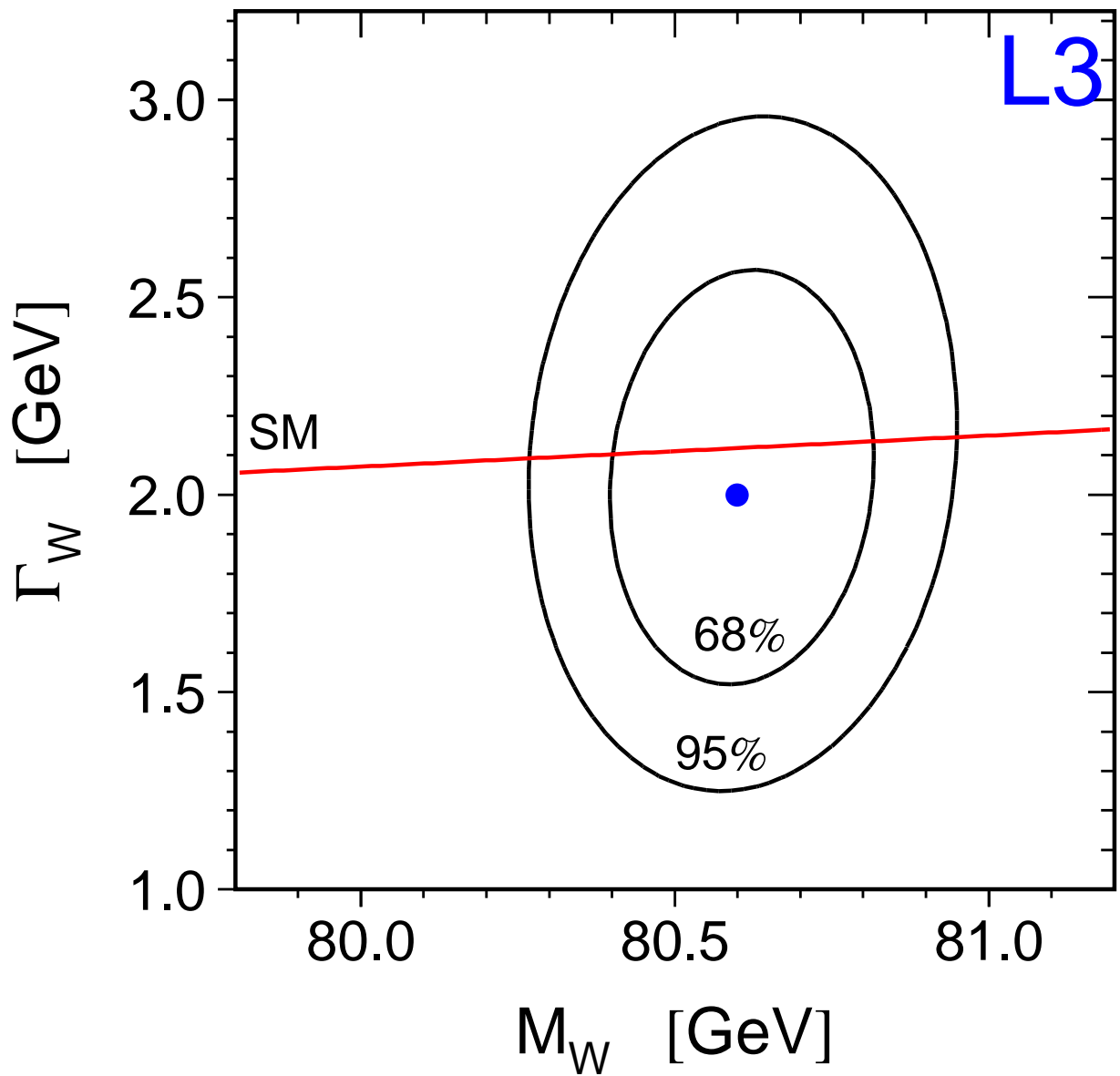


Figure 5: Contour curves of 68% and 95% probability in the (M_W, Γ_W) plane from a fit to the combined 172 GeV data and 183 GeV data (statistical errors only). The point represents the central values of the fit. The Standard Model dependence of Γ_W on M_W is shown as the line.